In situ calibration of an extreme ultraviolet spectrometer for attosecond transient absorption experiments

Xiaowei Wang,[1,2] Michael Chini,[2] Yan Cheng,[2] Yi Wu,[2] and Zenghu Chang[2,*]

[1]Department of Physics, National University of Defense Technology, Changsha, Hunan 410073, China

[2]CREOL and Department of Physics, University of Central Florida, Orlando, Florida 32816, USA

*Corresponding author: Zenghu.Chang@ucf.edu

Received 22 October 2012; accepted 7 December 2012;
posted 11 December 2012 (Doc. ID 177943); published 11 January 2013

We report a method for calibrating an extreme ultraviolet spectrometer based on a flat-field grazing incidence spherical grating in the energy range of 20–30 eV. By measuring absorption lines corresponding to singly excited states in helium atoms and autoionizing states in argon atoms, the photon energy of the detected light was determined. The spectral resolution of the spectrometer, 60 meV, was obtained by deconvolving the Fano resonance profile of argon autoionizing states from the measured absorption line profiles. © 2013 Optical Society of America

OCIS codes: 340.7480, 020.2649.

1. Introduction

With subcycle gating methods [1], high-order harmonic generation (HHG) is capable of producing single isolated pulses down to 67 as [2], which hold the promise of observing and controlling electron dynamics in atoms, molecules, and condensed matter. Recently, the attosecond transient absorption technique has been developed to take advantage of the broadband, continuous extreme ultraviolet (XUV) spectrum of such pulses [3–5]. In attosecond transient absorption measurements, the spectrum of the XUV pulse transmitted through an optically dense target is measured as a function of the time delay between the XUV attosecond pulse and a relatively strong near-infrared (NIR) laser pulse. The laser-induced electron dynamics of the target are then encoded in the transmitted XUV spectrum, as the absorption line positions, widths, and absorption strengths are modified on the few- and subfemtosecond timescales. It is therefore obvious that the accuracy and resolution of the XUV spectrometer plays a critical role in attosecond transient absorption experiments.

Generally, an XUV spectrometer consists of a grazing incidence flat-field grating (FFG) and a flat detector—either an XUV charge-coupled device (CCD) or a microchannel plate (MCP) and phosphor screen. To focus different wavelength components on a flat plane, the XUV grating is manufactured to have a spherical surface with variable groove spacing. Due to the complex structure of the grating, the image distance of each spectrum component is sensitive to the incidence angle and the distance between the object, typically chosen to be the target in transient absorption experiments, and the center of grating (object distance). Therefore, careful assembly and alignment is required to develop an XUV spectrometer with good performance. However, one cannot guarantee that all parameters in the real setup are precisely set to the designed values; and accurate calibration is necessary to appraise and optimize the XUV spectrometer.

XUV spectrometers are typically calibrated using the absorption edges of metal foils [6,7], laser-produced plasma lines [8,9], or electron-beam ion-trap (EBIT)

1559-128X/13/030323-07$15.00/0

emissions [10,11]. However, metal foils can provide only a few spectral features to benchmark the XUV spectrometer. On the other hand, the spectrum of XUV generated from plasma is generally very complicated, and generation of strong plasma lines requires much higher laser intensity than for HHG. EBIT is simply not available for most laboratories. Here, we report a convenient and accurate *in situ* method to calibrate an XUV spectrometer in the energy range of 20–30 eV (40–62 nm) for attosecond transient absorption experiments. The calibration was performed by measuring absorption lines corresponding to argon $3s3p^6np$ autoionizing states and helium 1snp excited states, with known photon energies lying between 20 and 30 eV. Furthermore, the argon autoionization lines with well-known Fano lineshapes [12,13] were used to determine the energy resolution of the spectrometer.

2. Experimental Setup

The attosecond transient absorption setup with a home-built XUV spectrometer is shown in Fig. 1. The 6 fs NIR laser pulses centered at 780 nm were split by a beam splitter (BS) into two parts; one of which was used to produce isolated attosecond pulses (IAPs) with the generalized double optical gating (GDOG) technique [14,15]. The GDOG optics consist of a quartz plate (QP) with optical axis set at 45° relative to the laser polarization axis, two thin Brewster windows (BW), a second QP with optical axis set along the laser polarization axis, and a β barium borate (BBO) crystal. IAPs with duration of ~140 as and central energy of 25 eV were generated from the first argon-filled gas cell (GC1). After being separated from the residual NIR laser by a 200 nm aluminum filter, the XUV beam was then focused by a toroidal mirror (TM, $f = 270$ mm) on a second gas cell (GC2) with inner diameter of 1 mm, which was filled with argon or helium gas. A hole-drilled mirror (HM) was placed between the TM and the GC2 to combine the dressing laser—the second part of the split NIR pulses—with the IAPs. In the dressing laser beam path, a delay-controlling mirror (DCM) that was set on a piezo stage was used to adjust the delay between IAPs and NIR laser pulses. After transmission through the second gas target, the IAPs were sent to the XUV spectrometer, in which the IAPs were dispersed by a grazing incidence FFG onto the MCP and finally recorded by a CCD camera with thermoeletric cooling.

The XUV spectrometer in our attosecond transient absorption setup was built to cover a spectrum range of 20–30 eV (40–62 nm). A Hitachi 001-0640 XUV grating with a flat spectrum range of 20–112 eV (11–62 nm) was adopted for the spectrometer, as shown in Fig. 2(a). The grating manufacturer's designed incidence angle α, object distance r, and image distance r' of the XUV grating are 85.3°, 350 mm, and 469 mm, respectively. Note that we do not have a slit in the spectrometer, since the XUV source size at the GC2 is small (~20 μm). The MCP surface was set to be parallel to the X axis in Fig. 2(a), which is defined as the normal of the grating surface.

Although the Hitachi 001-0640 XUV grating is specified as a FFG, not all the spectrum components in the range of 11–62 nm can be perfectly focused on a flat plane. In Fig. 2(b), focal "planes" of six different incidence angles are plotted for an IAP with a spectrum range from 11 nm (triangles) to 62 nm (squares). The 40 nm components (circles) are also marked in each focal plane. The Z axis in the figure is defined in Fig. 2(a) (parallel to the grating surface), and the MCP surface is parallel to the vertical grid lines (X axis). When the incidence angle is 85.3°, only 11–40 nm spectrum components are focused on a plane parallel to the MCP, while the focus of the spectrum components of 40–62 nm, which is the measuring range of the spectrometer, are on a curved surface. However, as shown in Fig. 2(b), an 86.5° incidence angle will result in a "flat" plane for the spectrum components of 40–62 nm, and the corresponding image distance is 448 mm. Those spectrum components can be focused on the MCP surface only by tuning the incidence angle and image distance.

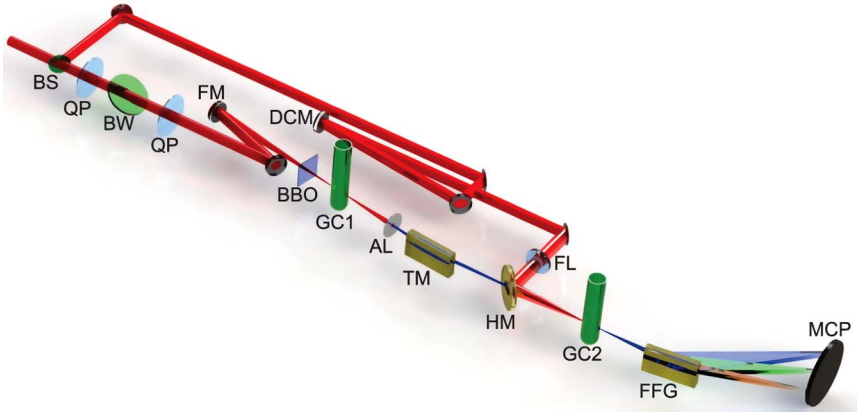

Fig. 1. (Color online) Schematic of experimental setup for attosecond transient absorption. BS, beam splitter; QP, quartz plate; BW, Brewster windows; FM, focusing mirror ($f = 500$ mm); DCM, delay-controlling mirror; GC1, argon-backed gas cell for IAP generation; AL, aluminum foil filter; TM, toroidal mirror ($f = 270$ mm); FL, focusing lens ($f = 400$ mm); HM, hole-drilled mirror; GC2, helium/argon-backed gas cell for absorption measurements; FFG, flat-field grating; MCP, microchannel plate and phosphor screen detector.

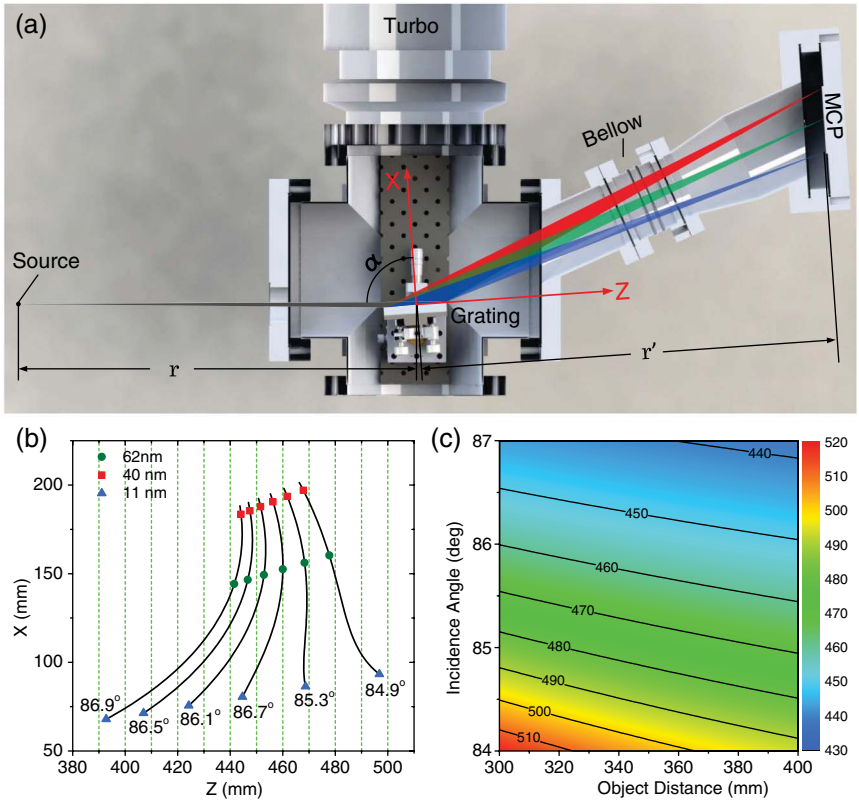

Fig. 2. (Color online) (a) Top view of the XUV spectrometer. (b) Focal "plane" of the XUV grating for different incidence angles. Each plane covers a spectrum range from 11 nm (triangles) to 62 nm (squares), and the 40 nm components (circles) are also marked in each focal plane. For 86.5° incidence angle, the spectrum from 40 to 60 nm is approximately in a vertical plane (MCP plane). The axes are defined in (a). (c) Dependence of grating image distance of 40 nm XUV light on object distance and incidence angle.

Furthermore, the image distance of the XUV grating is sensitive to the incidence angle and object distance. In Fig. 3(c), we calculated the image distance of the XUV grating for different incidence angles and object distances. The wavelength of the incidence light is assumed to be 40 nm. The result shows that 2 cm error in the object distance will give rise to a deviation of the image distance by 5 mm, and a 0.5° error in the incidence angle will lead to a 10 mm image distance deviation. These errors will dramatically enlarge the spatial dimension of the line spectrum on the MCP detector, which worsens the resolution of the spectrometer. Therefore to achieve high resolution, we made the incidence angle and image distance adjustable in our setup. The grating was held by a mirror mount with actuators connected to rotary feedthroughs on the side flange of the vacuum chamber. This design allows fine tuning of the grating even when the spectrometer is under vacuum. The dispersed XUV spectrum reaches the MCP after passing through an extension tube and a bellow, which makes the image distance r' adjustable in the range of 440–470 mm.

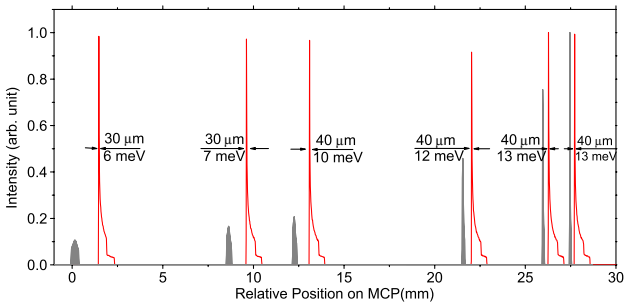

Fig. 3. (Color online) Profile of the focused spectrum on the MCP when the incidence angle is set to be 85.3° (gray-filled) and 86.5° (red solid curve). The six peaks (from left to right) are spectral lines located at the known energies of the helium 1s2p, 1s3p, and 1s4p absorption lines and argon 3s3p64p, 3s3p65p, and 3s3p66p autoionization lines, respectively. Both spatial and spectral FWHM is labeled for each peak with 86.5° incidence angle.

Since the grating in our setup is not being used with its manufacturer's design parameters, ray tracing was carried out with Zemax [16] to verify the resolution under our preferred geometric configuration, i.e., 86.5° incidence angle and 448 mm imaging distance. The light source in the ray tracing is a point source consisting of six different wavelength components corresponding to three helium absorption lines (1s2p, 1s3p, and 1s4p) and three argon autoionization lines ($3s3p^64p$, $3s3p^65p$, and $3s3p^66p$). In Fig. 3, the spatial profiles of the focused spectrum on the MCP with factory-designed (gray-filled area) and preferred (solid curve) incidence angle and image distance are presented. A small offset of the horizontal position of the solid curve was introduced, to avoid spectral overlap in the figure. The position axis is along the MCP surface, and the corresponding photon

energy increases as the position axis increases. Therefore, the left three peaks represent the energies of the helium absorption lines and the right three represent the argon autoionization lines. We can see that the spatial width of the focused spectrum with the factory-designed incidence angle is quite large except for the high-energy spectrum components, but with the incidence angle and image distance optimized for the 20–30 eV spectral range, the spatial full width at half-maximum (FWHM) of each spectrum peak can be reduced to 30–40 μm in the entire energy range of the spectrometer. Since the spatial resolution of the MCP imager is larger than 30 μm, this indicates that the grating will not be the limiting factor in the final instrument resolution. By taking into account the reciprocal linear dispersion of the grating, we can also estimate the spectral FWHM, which is equivalent to the lower limit of the spectrometer resolution. The spectrometer resolution is found to be approximately 10(±4) meV, as labeled in Fig. 3, and becomes slightly worse with increasing photon energy.

During the calibration experiments, the transmitted XUV spectra after absorption by both helium and argon gas were measured. The ionization potential of helium (24.6 eV) is within the spectrometer energy range, so a step-like absorption threshold is expected. Further, the excitation of 1snp bound states of helium will leave its mark in the measured absorption spectrum. Without external disturbance to the atom, the 1snp excitation state lifetimes can be as long as several nanoseconds [17], corresponding to nano-eV linewidths in the spectrum. One would think that such a narrow absorption line (like a delta function) is perfect for calibrating the spectral resolution. However, such narrow features could not be observed experimentally since the limited resolution also results in a reduction of the absorption peak height. In order to observe these absorption lines, a delayed, moderately intense ($\sim 10^{12}$ W/cm^2) NIR laser pulse was focused to the second cell to dress the helium atoms. Due to few-photon ionization of the delayed NIR field, the lifetime can be reduced to the femtosecond timescale, leading to broadened energy resonances and increased absorption. Note that the negative delay between NIR and XUV (XUV pulses arrive at the second cell first) will result in more clear absorption lines than positive delay due to the delayed ionization of the 1snp states, while AC stark shifts of the energy levels of helium bound states strongly modify the energies near the zero delay [5]. Therefore, the XUV spectrometer should be calibrated with negative delay between the NIR and XUV pulses for helium gas.

The ionization potential of argon is 15.7 eV, which is much lower than the energy range of the spectrometer. Thus, all the measured spectrum components will be strongly absorbed due to single-photon photoionization [18]. However, several core-excited autoionizing states of argon lie within the energy range of the spectrometer [4,12], and the interference between the direct ionization and the autoionization results in Fano resonance profiles [19], which can be observed as transmission peaks in the absorption spectrum. The linewidths of the 3s3p^{6}4p, 3s3p^{6}5p, and 3s3p^{6}6p states of argon are 80, 28.2, and 12.6 meV, respectively, which are comparable to the anticipated resolution of the XUV spectrometer. Therefore, the linewidth of the measured argon absorption spectrum should be larger than the spectrometer resolution, since the measured absorption cross section $\sigma_{\mathrm{exp}}(E)$ is the result of the Fano resonance profiles convoluted by the spectrometer response function [20,21]:

$$\sigma_{\mathrm{exp}}(E) = \sigma(E) * G(E), \tag{1}$$

where $\sigma(E)$ is the Fano resonance profile of argon autoionization states, and $G(E)$ can be considered as a Gaussian function with FWHM equal to the spectrometer resolution δE:

$$G(E) = \exp\left(-4\ln(2)\frac{E^2}{\delta E^2}\right). \tag{2}$$

The spectrometer resolution can then be obtained by deconvolving the Fano resonance profiles of argon autoionizing states, which are well known [12,13], from the measured spectrum. This method is accurate since the measured spectrum lines have linewidths comparable to the spectrometer resolution.

3. Result and Discussion

The transmission of XUV pulses after passing through the argon and helium gases is presented in Fig. 4(a). The backing pressure of the second cell

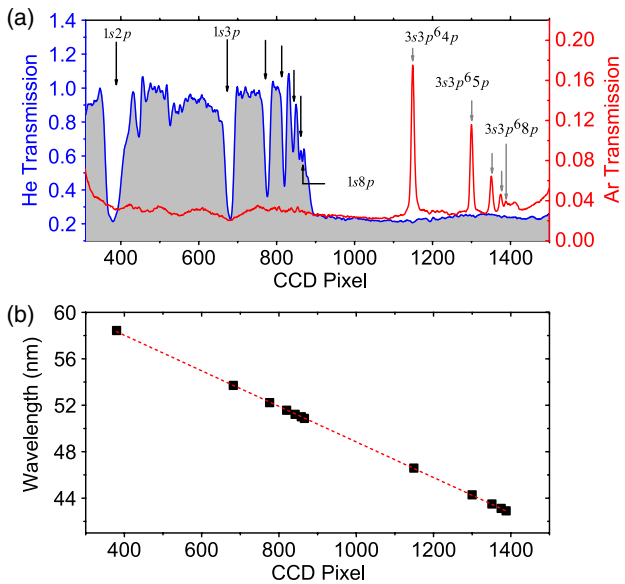

Fig. 4. (Color online) (a) Transmission of XUV pulses through a 35 torr argon cell (red solid curve) or a 50 torr helium cell (blue curve with filled area). Five argon autoionization peaks and seven helium absorption dips are identified in the figure. (b) Wavelengths of the 12 spectral lines (squares) identified in (a), and the linear fitting (red dashed line).

was 35 and 50 torr for argon and helium, respectively. In the argon transmission curve (red solid), five peaks corresponding to the five autoionizing states listed in Table 1 are identified by the gray arrows. In the helium absorption experiment, the delay and intensity of the dressing laser were set to be approximately −40 fs and 5×10^{12} W/cm^2, respectively, to broaden the 1snp absorption lines. The step around the 900th pixel in the helium transmission curve (blue curve with filled area) corresponds to the ionization potential of helium. Below the ionization potential, only those photons with energy equal to the dressed 1snp excited states could be strongly absorbed due to transitions from the ground state to the corresponding excited states. Absorption lines below the 900th pixel (black arrows) indicate the position of helium 1snp excited states. Between the 1s2p and 1s3p states, there are several smaller absorption features, which are caused by two-color two-photon (XUV+NIR) absorption to corresponding "s" and "d" states. All spectrum lines we used to calibrate the XUV spectrometer are listed in Table 1.

We have 12 known spectral lines with which to calibrate the spectrometer. The known wavelengths of the spectrum lines are plotted in Fig. 4(b) as a function of their pixel location on the CCD. In the narrow wavelength range of interest it is a reasonable assumption that the wavelength is proportional to pixel position, and the relationship between the wavelength and pixel location can be fit as

$$\lambda = kx + \lambda_0. \tag{3}$$

By performing linear least-square fitting for the 12 known spectral lines, as shown by the dashed line in Fig. 4(b), we obtain $k = -0.01531$ nm/pixel and $\lambda_0 = 64.154$ nm. The effective pixels of XUV spectrum on the CCD are in the range of 310–1500, so the wavelength range of the spectrometer is 41.19–59.41 nm (20.87–30.10 eV). After the calibration of the spectrometer, we can easily measure the FWHM of each spectrum line by fitting the spectrum line with a Gaussian curve. The FWHM of each spectral line is listed in Table 1 (some peaks are too weak to be correctly fit). The narrowest spectrum lines we can observe are 69.5 meV at 24 eV in helium and 81 meV at 28 eV in argon, which place an upper limit on the spectrometer resolution since we do not know the actual linewidth of the helium 1snp excited states in the presence of the NIR dressing laser and the argon absorption lines have non-Gaussian Fano profiles.

Table 1. Spectrum Lines Used to Calibrate the Spectrometer

States		Energy (eV) [12,22]	Measured linewidth FWHM (meV)
He	1s2p	21.242	235.9
	1s3p	23.113	144.3
	1s4p	23.769	86.4
	1s5p	24.073	69.7
	1s6p	24.239	69.5
	1s7p	24.338	—
	1s8p	24.403	—
Ar	$3s3p^64p$	26.646	82.46
	$3s3p^65p$	28.023	81.02
	$3s3p^66p$	28.543	82.3
	$3s3p^67p$	28.793	81.7
	$3s3p^68p$	28.933	—

The spectrometer resolution could be obtained by a deconvolution of the Fano profile and the measured spectrum line profiles with argon gas according to Eq. (1). Theoretically, $G(E)$ can be easily determined by performing the Fourier transform of Eq. (1), but experimental error and the small energy range makes this method impractical. Instead, we found the spectrometer resolution δE by minimizing the following error function:

$$f(\delta E) = \sum_E |\sigma_{\exp}(E) - \sigma(E) * G(E)|^2, \tag{4}$$

where $\sigma_{\exp}(E)$ is the measured absorption cross section, which is related to the measured transmission $T(E)$ by $\sigma_{\exp}(E) \propto -\ln(T(E))$, and $\sigma(E)$ is made up of the overlapping Fano profiles of several argon autoionization states and takes the form [19,20]

$$\sigma(E) = \sum_i a_i \frac{(q_i + \varepsilon_i)^2}{1 + \varepsilon_i^2} + b, \qquad \varepsilon_i = \frac{E - Er_i}{\Gamma_i/2}, \tag{5}$$

where each autoionization state is characterized by its resonance energy Er_i, its width Γ_i, and the q_i parameter that determines the shape of the resonance.

We used the first three argon autoionization states, i.e., $3s3p^64p$, $3s3p^65p$, and $3s3p^66p$, whose Fano parameters are listed in Table 2. In the error function, a_i, b, and spectrometer resolution δE are the parameters to be fitted. The spectrometer resolution was found to be $\delta E = 60$ meV by minimizing the error function in Eq. (4). Figure 5 shows the convolution result (solid curve) between overlapped Fano resonance profile of the first three argon autoionization states and the Gaussian response function with FWHM of 60 meV, as well as our measured absorption cross section (dots). As we can see, the calculated absorption cross section is consistent with the experimental data, which indicates that our calculated spectrometer resolution is reasonably accurate.

Although the ray-tracing result suggests a resolution as high as 10 meV, the resolution of our XUV spectrometer is calibrated to be 60 meV. The difference is mainly caused by the transverse

Table 2. Fano Parameters for the First Three Peaks of Ar $3s3p^6np$ Autoionizing States [12]

State	Er (eV)	Γ (meV)	q
$3s3p^64p$	26.614	80	−0.22
$3s3p^65p$	28.023	28.2	−0.21
$3s3p^66p$	28.543	12.6	−0.17

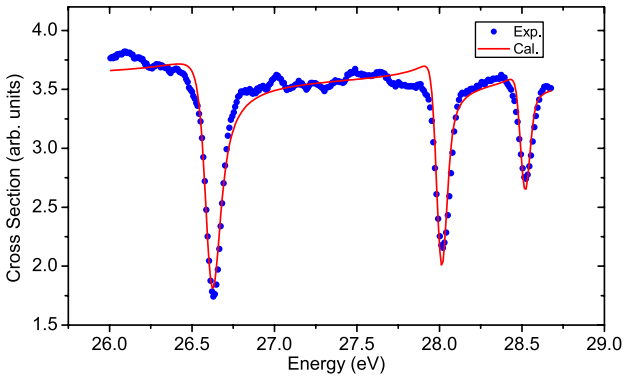

Fig. 5. (Color online) Comparison between measured absorption cross section (dots) and argon autoionization Fano profile convoluted by a Gaussian function with FWHM of 60 meV (solid curve).

displacement of electrons from the MCP to the phosphor [23,24] and the spatial resolution of the CCD camera. To determine the resolution of our imaging system, we measured the phosphor emission corresponding to the so-called "quantum noise." When a sufficiently high voltage is applied to the front surface of the MCP, a stray electron arising in a microchannel will be multiplied and form an electron avalanche. The observed phosphor emission can then be considered to arise from an electron in a single microchannel pore, giving the ultimate energy resolution of the imaging system. Figure 6 shows the image of quantum noise from one microchannel, along with the lineouts in the x (spectrum) and y (position) axes. The FWHM of the image is 131(±27) and 151(±33) μm along x and y axes, respectively, which were obtained by performing a Gaussian fit (solid curve) to the measured distributions (symbols). The FWHM errors are about one

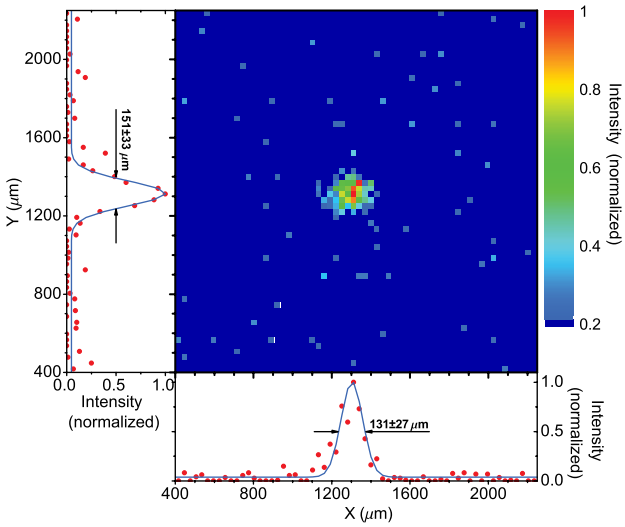

Fig. 6. (Color online) Image of the electron distribution of a single microchannel pore, with corresponding lineouts (symbols) along the x (dispersion) and y (position) axes. Gaussian fits (solid curve) to the measured distribution give FWHM resolution of 131(±27) μm and 151(±33) μm along the x and y axes, respectively. The error comes from the Gaussian fit.

pixel on the CCD that corresponds to 29.8 μm on the phosphor. According to the dispersion relation in Eq. (3), our spectrometer resolution of 60 meV corresponds to 190(±13) μm in the energy region of the three argon autoionization states, which is consistent with the measured electron distribution if we take into account the asymmetric distribution of the line-spread function shown in Fig. 3 and the approximations in the deconvolution. Therefore, our spectrometer resolution is primarily limited by the MCP imaging resolution.

4. Conclusions

In conclusion, we implemented a novel method to calibrate an XUV spectrometer with an energy range of 20–30 eV for attosecond transient absorption experiments. By measuring laser-dressed helium absorption lines and argon autoionization lines, the XUV spectrometer was easily calibrated *in situ*. Twelve known spectral features within the spectrometer energy range were used to improve the reliability and accuracy of the calibration. The spectral resolution was determined by deconvolving the well-known argon autoionization Fano profile from the measured spectrum. The linewidths of argon autoionization lines are comparable to the spectrometer resolution, which assures the accuracy of the deconvolution. By choosing different absorption gases, the reported method is capable of calibrating spectrometers working in other energy ranges or with other XUV sources with sufficient bandwidth.

This material is supported by the U.S. Army Research Office and the National Science Foundation.

References

1. Z. Chang and P. Corkum, "Attosecond photon sources: the first decade and beyond [Invited]," J. Opt. Soc. Am. B **27**, B9–B17 (2010).
2. K. Zhao, Q. Zhang, M. Chini, Y. Wu, X. Wang, and Z. Chang, "Tailoring a 67 attosecond pulse through advantageous phase-mismatch," Opt. Lett. **37**, 3891–3893 (2012).
3. E. Goulielmakis, Z.-H. Loh, A. Wirth, R. Santra, N. Rohringer, V. S. Yakovlev, S. Zherebtsov, T. Pfeifer, A. M. Azzeer, M. F. Kling, S. R. Leone, and F. Krausz, "Real-time observation of valence electron motion," Nature **466**, 739–743 (2010).
4. H. Wang, M. Chini, S. Chen, C.-H. Zhang, F. He, Y. Cheng, Y. Wu, U. Thumm, and Z. Chang, "Attosecond time-resolved autoionization of argon," Phys. Rev. Lett. **105**, 143002 (2010).
5. M. Chini, B. Zhao, H. Wang, Y. Cheng, S. X. Hu, and Z. Chang, "Sub-cycle AC Stark shift of helium excited states probed with isolated attosecond pulses," Phys. Rev. Lett. **109**, 073601 (2012).
6. M. Fieβ, M. Schultze, E. Goulielmakis, B. Dennhardt, J. Gagnon, M. Hofstetter, R. Kienberger, and F. Krausz, "Versatile apparatus for attosecond metrology and spectroscopy," Rev. Sci. Instrum. **81**, 093103 (2010).
7. Z.-H. Loh, M. Khalil, R. E. Correa, and S. R. Leone, "A tabletop femtosecond time-resolved soft x-ray transient absorption spectrometer," Rev. Sci. Instrum. **79**, 073101 (2008).
8. N. Nakano, H. Kuroda, T. Kita, and T. Harada, "Development of a flat-field grazing-incidence XUV spectrometer and its application in picosecond XUV spectroscopy," Appl. Opt. **23**, 2386–2392 (1984).

9. J. P. Farrell, B. K. McFarland, P. H. Bucksbaum, and M. Gühr, "Calibration of a high harmonic spectrometer by laser induced plasma emission," Opt. Express **17**, 15134–15144 (2009).
10. B. Blagojevic, E.-O. Le Bigot, K. Fahy, A. Aguilar, K. Makonyi, E. Takács, J. N. Tan, J. M. Pomeroy, J. H. Burnett, J. D. Gillaspy, and J. R. Roberts, "A high efficiency ultrahigh vacuum compatible flat field spectrometer for extreme ultraviolet wavelengths," Rev. Sci. Instrum. **76**, 083102 (2005).
11. J. Park, G. V. Brown, M. B. Schneider, H. A. Baldis, P. Beiersdorfer, K. V. Cone, R. L. Kelley, C. A. Kilbourne, E. W. Magee, M. J. May, and F. S. Porter, "Calibration of a flat field soft x-ray grating spectrometer for laser produced plasmas," Rev. Sci. Instrum. **81**, 10E319 (2010).
12. R. P. Madden, D. L. Ederer, and K. Codling, "Resonances in the photo-ionization continuum of Ar I (20–150 eV)," Phys. Rev. **177**, 136–151 (1969).
13. J. W. McConkey and J. A. Preston, "Autoionizing states in argon," J. Phys. B **6**, L138–L141 (1967).
14. H. Mashiko, S. Gilbertson, C. Li, S. D. Khan, M. M. Shakya, E. Moon, and Z. Chang, "Double optical gating of high-order harmonic generation with carrier-envelope phase stabilized lasers," Phys. Rev. Lett. **100**, 103906 (2008).
15. X. Feng, S. Gilbertson, H. Mashiko, H. Wang, S. D. Khan, M. Chini, Y. Wu, K. Zhao, and Z. Chang, "Generation of isolated attosecond pulses with 20 to 28 femtosecond lasers," Phys. Rev. Lett. **103**, 183901 (2009).
16. http://www.radiantzemax.com/en/zemax/.
17. M. Žitnik, A. Stanič, K. Bučar, J. G. Lambourne, F. Penent, R. I. Hall, and P. Lablanquie, "Lifetimes of n^1p states in helium," J. Phys. B **36**, 4175–4189 (2003).
18. http://www.cxro.lbl.gov/.
19. U. Fano, "Effects of configuration interaction on intensities and phase shifts," Phys. Rev. **124**, 1866–1878 (1961).
20. T. K. Fang and T. N. Chang, "Determination of profile parameters of a Fano resonance without an ultrahigh-energy resolution," Phys. Rev. A **57**, 4407–4412 (1998).
21. X. Liu, Y. Huang, L. Zhu, Z. Yuan, W. Li, and K. Xu, "Numerical determination of profile parameters for fano resonance with definite energy resolution," Nucl. Instrum. Methods Phys. Res. A **508**, 448–453 (2003).
22. G. W. F. Drake, ed., *Springer Handbook of Atomic, Molecular and Optical Physics*, (Springer, 2006).
23. Y. Cheng, "A first step towards intense single attosecond pulse generation from 400 nm driving laser," master's thesis (Kansas State University, 2011).
24. A. S. Tremsin and O. H. W. Siegmund, "Spatial distribution of electron cloud footprints from microchannel plates: measurements and modeling," Rev. Sci. Instrum. **70**, 3282–3288 (1999).